Nonlinear Dyn (2012) 69:495–509
DOI 10.1007/s11071-011-0280-3

ORIGINAL PAPER

Global stabilization of 2-DOF underactuated mechanical systems—an equivalent-input-disturbance approach

Jinhua She · Ancai Zhang · Xuzhi Lai · Min Wu

Received: 13 June 2011 / Accepted: 21 October 2011 / Published online: 4 January 2012

Abstract This paper presents a new method of globally stabilizing a non-linear underactuated mechanical system with two degrees of freedom (DOF). It is based on the idea of equivalent input disturbance (EID), and designing the controller requires only the state variables of position, not velocity. The design procedure has two steps: (1) Use a global homeomorphic coordinate transformation to convert the original system into a new non-linear system. This changes the problem of stabilizing the original system into one of stabilizing the new system. (2) Divide the new system into linear and non-linear parts and take the non-linear part to be an artificial disturbance, thereby enabling use of the EID approach to globally asymptotically stabilize the new system at the origin. The new method was tested through numerical simulations on three well-known 2-DOF underactuated mechanical systems (TORA, beam ball, inertia wheel pendulum). The results demonstrate its validity and its superiority over others.

J. She · A. Zhang · X. Lai (✉) · M. Wu
School of Information Science and Engineering, Central South University, Changsha, Hunan 410083, China
e-mail: xuzhi@csu.edu.cn

J. She · A. Zhang
School of Computer Science, Tokyo University of Technology, Hachioji, Tokyo 192-0982, Japan

Keywords Equivalent input disturbance (EID) · Global asymptotical stabilization · Non-holonomic constrain · Underactuated mechanical system

1 Introduction

An underactuated mechanical system is a system that has fewer actuators than degrees of freedom (DOF). Spacecraft, underwater vehicles, mobile robots, surface vessels, and many other systems have this characteristic. Since systems of this type are lighter and less energy-consuming than fully-actuated ones, they are used extensively in the fields of aerospace, transportation, and industrial manufacturing; and there is increasing interest in the problem of controlling their motion [1–3].

The simplest type of underactuated mechanical system is a 2-DOF system with one control input. Examples include a translational oscillator with rotational actuator (TORA) [4], a two-link underactuated manipulator [5, 6], a beam–ball system [7], a Furuta pendulum [8], and an inertia wheel pendulum [9]. This type of system exhibits strong non-linearities. Moreover, since one degree of freedom is passive, a second-order non-holonomic constraint is usually imposed [10]. This makes control of such systems a challenging task.

Over the last couple of decades, a number of methods have been developed to solve the problem of stabilizing a 2-DOF underactuated system. The most used

approach is the energy-based (EB) method in [11] that utilized energy passivity in the design of a stabilizing controller. It has been applied to many underactuated mechanical systems [12–14]. In addition, since most underactuated systems are not full-state feedback linearizable [15], attempts have been made to transform an underactuated system into a new system that has a partially linear structure [16–18]. One example is the partial feedback linearization (PFL) method of [16], which linearizes one of the actuated or un-actuated parts and uses a transformation on the control input to achieve the control objective. But the appearance of the new control input in both the actuated and un-actuated parts of the transformed system complicates the design of a PFL-based control system. The main feature of both the EB and PFL methods is the requirement of designing of a couple of different controllers and using an integration or switching strategy to coordinate them. As a result, they do not usually guarantee the global stability of the control system. To solve this problem, the backstepping (BS)-based method of [19] introduces new variables into the original system. Although it only requires a single controller to stabilize the system, the control law is very complicated for two reasons: This method suffers from the problem of the explosion of terms, and it sometimes requires the explicit solution of highly nonlinear equations. The dynamic surface control (DSC) method of [20] overcomes these shortcomings by using a low-pass filter, but it lacks theoretical rigor. Other approaches to the stabilization of a 2-DOF underactuated system include energy reshaping [21], the construction of fictitious output [22], and sliding-mode control [23]. However, all of them require full state information (positions and velocities) for the design of a control law. This is also true of the EB, PFL, BS, and DSC methods.

Generally speaking, the position can be accurately measured with an encoder. However, since velocity is generally measured with a tachometer, it usually contains noise, which can affect the control performance of the system. Moreover, the installation of a tachometer increases the cost of the control system. So, it is meaningful from both practical and theoretical viewpoints to stabilize a mechanical system using only position measurements. For a fully actuated mechanical system, researchers have successfully achieved this goal by using observer- based design methods (for example, [24]). However, this strategy is difficult to extend to an underactuated system due to the reduction of the dimension of the control input and the complexity of the dynamics. Devising a method of stabilizing an underactuated system that relies only on the measurement of positions is still a challenging problem.

In this study, we categorized 2-DOF underactuated systems into three types and developed a new nonlinear control method that uses only positional information to globally asymptotically stabilize them at the origin. Our method is based on the idea of equivalent input disturbance (EID), which was first presented in [25] to deal with disturbance rejection in a linear servo system. This study extends the concept to the stabilization of 2-DOF underactuated non-linear mechanical systems. The design procedure has two steps: (1) Use a global homeomorphic coordinate transformation to transform the system into a new nonlinear system that is easier to handle. (2) Divide the new system into a linear and a non-linear part, take the non-linear part to be an artificial disturbance, and use the EID-based approach to compensate for that disturbance so as to globally stabilize the new system at the origin.

The rest of this paper is organized as follows. Section 2 presents a dynamic model of a 2-DOF underactuated system. Section 3 describes a coordinate transformation for the original underactuated system. Section 4 explains the design of an EID-based stabilizing control law. Section 5 presents some numerical examples for three typical 2-DOF underactuated systems. Finally, Sect. 6 presents some concluding remarks.

2 System modeling

Let q_1 and q_2 be the configuration variables for the un-actuated and actuated parts, respectively, of a 2-DOF underactuated mechanical system; and let $q = [q_1, q_2]^T$. Choose the Lagrangian of the system to be

$$L(q, \dot{q}) = \frac{1}{2}\dot{q}^T M(q)\dot{q} - P(q) \tag{1}$$

where $\dot{q} = dq/dt$, $P(q)$ is the potential energy of the system, and $M(q) \in \mathbb{R}^{2\times 2}$ is a positive-definite symmetric inertia matrix. The general form of $M(q)$ is

$$M(q) = \begin{bmatrix} m_{11}(q) & m_{12}(q) \\ m_{21}(q) & m_{22}(q) \end{bmatrix} \tag{2}$$

The dynamic equation is obtained from the Euler–Lagrange equations:

$$\frac{d}{dt}\left[\frac{\partial L(q,\dot{q})}{\partial \dot{q}_1}\right] - \frac{\partial L(q,\dot{q})}{\partial q_1} = 0 \tag{3a}$$

$$\frac{d}{dt}\left[\frac{\partial L(q,\dot{q})}{\partial \dot{q}_2}\right] - \frac{\partial L(q,\dot{q})}{\partial q_2} = \tau_2 \tag{3b}$$

where τ_2 is the control input applied to variable q_2, which is for the actuated part. We rewrite (3a)–(3b) in the general form

$$M(q)\ddot{q} + C(q,\dot{q}) + G(q) = \begin{bmatrix} 0 \\ \tau_2 \end{bmatrix} \tag{4}$$

where $C(q,\dot{q}) = [C_1(q,\dot{q}), C_2(q,\dot{q})]^T$ is the combination of the Coriolis and centrifugal forces; $G(q) = [G_1(q), G_2(q)]^T$ contains the effects of gravity and elasticity; and

$$G(q) = \frac{\partial P(q)}{\partial q} \tag{5}$$

Note that, for an underactuated system, the number of control inputs is less than the number of generalized coordinates. As a result, many underactuated systems are not full-state feedback linearizable (FL), and some are not even small-time locally controllable (STLC) [26]. This characteristic of the system is revealed by the zero term on the right side of (3a), which indicates that there are no exogenous control signals input on the subsystem (3a). As pointed out in [10], this second-order differential equation is not integrable when the term $G(q)$ is not constant. Some researchers call (3a) a second-order non-holonomic constraint to make this point clear.

We categorize underactuated systems into three types according to the characteristics of the inertia matrix. When the inertia matrix is constant, we have the first class:

(1) An underactuated system with constant inertia matrix (USCIM), that is, $M(q) = M_0$. An example of a 2-DOF USCIM is an inertia wheel pendulum.

When the inertia matrix is not constant, the configuration variables that appear in it are called shape variables. The classifications for this type are based on whether the shape variable is for the actuated or the unactuated part:

(2) An underactuated system with a shape variable for the actuated part (USSV-A), that is, $M(q) = M(q_2)$. Examples include an acrobot and a TORA.
(3) An underactuated system with a shape variable for the unactuated part (USSV-U), that is, $M(q) = M(q_1)$. Examples include a beam–ball system, a pendubot, a rotating pendulum, and a cart pendulum.

This study considered the problem of globally stabilizing these three kinds of systems under the assumption that only the position, q, is known.

3 Coordinate transformation

For the non-linear system (4), although the input only appears on the actuated part, it influences the unactuated part due to the coupling of the inertia matrix. This makes the stabilization of (4) difficult. To make the analysis and design of the control system easy, we introduce a coordinate transformation that transforms the original system into a simple cascade nonlinear system. Equation (3a) shows that the first derivative of the term, $\partial L(q,\dot{q})/\partial \dot{q}_1$, with respect to time is related only to q and $\dot{q}$, but not to $\ddot{q}$. Based on this property and the partial feedback linearization method [16], we have a global coordinate transformation for (4):

$$\mathcal{T}: \quad \begin{cases} z_1 = q_1 + \alpha(q_2) \\ z_2 = \frac{\partial L(q,\dot{q})}{\partial \dot{q}_1} = m_{11}(q)\dot{q}_1 + m_{12}(q)\dot{q}_2 \\ z_3 = q_2 \\ z_4 = \dot{q}_2 \end{cases} \tag{6}$$

where $\alpha(\cdot)$ is a continuous function and $\alpha(0) = 0$. Let Γ be the Jacobian matrix of the transformation from $\zeta = [q_1, q_2, \dot{q}_1, \dot{q}_2]^T$ to $z = [z_1, z_2, z_3, z_4]^T$, that is, $\Gamma = \partial z/\partial \zeta^T$. It is easy to show that $\det[\Gamma] = -m_{11}(q) < 0$. So, $\mathcal{T}$ is a homeomorphic transformation. From (6), we obtain the inverse transformation of $\mathcal{T}$:

$$\mathcal{T}^{-1}: \quad \begin{cases} q_1 = z_1 - \alpha(z_3) \\ q_2 = z_3 \\ \dot{q}_1 = \frac{z_2 - m_{12}(q)z_4}{m_{11}(q)}\Big|_{q_1 = z_1 - \alpha(z_3), q_2 = z_3} \\ \dot{q}_2 = z_4 \end{cases} \tag{7}$$

Combining (3), (4), (5), and (6) yields a new dynamic equation for a 2-DOF underactuated system in the

z-state:

$$\begin{cases} \dot{z}_1 = f_1(z) \\ \dot{z}_2 = f_2(z) \\ \dot{z}_3 = z_4 \\ \dot{z}_4 = u \end{cases} \tag{8}$$

or

$$\dot{z} = f(z) + Bu \tag{9}$$

where

$$f_1(z) = \left[\frac{z_2}{m_{11}(q)} + \left(\frac{d\alpha(q_2)}{dq_2} - \frac{m_{12}(q)}{m_{11}(q)} \right) z_4 \right] \Bigg|_{\zeta = \mathcal{T}^{-1}(z)} \tag{10}$$

$$f_2(z) = \left[\frac{1}{2} \dot{q}^T \frac{\partial Mq}{\partial q_1} \dot{q} - G_1(q) \right] \Bigg|_{\zeta = \mathcal{T}^{-1}(z)} \tag{11}$$

$$f(z) = \left[f_1(z),\ f_2(z),\ z_4,\ 0 \right]^T \tag{12}$$

$$B = [0,\ 0,\ 0,\ 1]^T \tag{13}$$

and u is the input of the new system. From (4), we obtain the relationship between u and τ_2:

$$\tau_2 = \frac{\det[M(q)]}{m_{11}(q)} u + C_2(q, \dot{q}) + G_2(q) - \frac{m_{21}(q)[C_1(q, \dot{q}) + G_1(q)]}{m_{11}(q)} \tag{14}$$

$$\det\left[M(q)\right] = m_{11}(q) m_{22}(q) - m_{12}(q) m_{21}(q) > 0 \tag{15}$$

To make $f_1(z)$ simple, we need to choose a different $\alpha(q_2)$ for a different type of a 2-DOF underactuated system. Specifically, it is suitable to choose

$$\alpha(q_2) = \int_0^{q_2} \frac{m_{12}(s)}{m_{11}(s)} ds \tag{16}$$

for a USSV-A, and to choose

$$\alpha(q_2) = 0 \tag{17}$$

for a USSV-U. We can choose $\alpha(q_2)$ to be (16) or (17) for a USCIM.

In addition, we note that the new control input, u, of the system (8) only drives z_4; and (8) is a cascade nonlinear system. The system structure of (8) is simpler than that of (4). It makes the problem of designing a controller that stabilizes a 2-DOF underactuated system easy to solve.

Since the transformation matrix is non-singular, $\zeta = 0$ is equivalent to $z = 0$. That means that global and asymptotic stabilization of the system (8) at $z = 0$ guarantees the global and asymptotic convergence of the system (4) at the origin. In other words, global stabilization control of the system (4) is guaranteed as long as there exists a control law, u, that globally stabilizes the system (8) at $z = 0$. The discussion below focuses on finding such a law.

4 Design of EID-based control law

This section explains how to use the concept of EID to design a stabilizing controller for the non-linear system (8).

First, we divide the right side of (9) into linear and nonlinear parts, take z_1 and z_3 to be the outputs of the system, and rewrite the dynamics of the system as

$$\begin{cases} \dot{z} = Az + Bu + \delta \\ y = Cz \end{cases} \tag{18}$$

where

$$A = \frac{\partial f(z)}{\partial z}^T \Bigg|_{z=0} = \begin{bmatrix} a_{11} & a_{12} & a_{13} & a_{14} \\ a_{21} & a_{22} & a_{23} & a_{24} \\ 0 & 0 & 0 & 1 \\ 0 & 0 & 0 & 0 \end{bmatrix},$$

$$a_{ij} = \frac{\partial f_i(z)}{\partial z_j} \Bigg|_{z=0} \tag{19}$$

$$C = \begin{bmatrix} 1 & 0 & 0 & 0 \\ 0 & 0 & 1 & 0 \end{bmatrix} \tag{20}$$

and $\delta := \Phi(z) = f(z) - Az$. From (8), (10), and (18), we know that $y = 0$ is equivalent to $z = 0$. Combining (10), (11), and (19) yields

$$\begin{cases} a_{11} = a_{13} = 0, \quad a_{22} = a_{24} = 0, \quad a_{12} = \frac{1}{m_{11}(0)} \\ a_{14} = \left[\frac{d\alpha(q_2)}{dq_2} - \frac{m_{12}(q)}{m_{11}(q)} \right]_{q=0}, \quad a_{21} = -\frac{\partial G_1}{\partial q_1}\Big|_{q=0} \\ a_{23} = \left[\frac{\partial G_1}{\partial q_1} \frac{d\alpha(q_2)}{dq_2} - \frac{\partial G_1}{\partial q_2} \right]_{q=0} \end{cases} \tag{21}$$

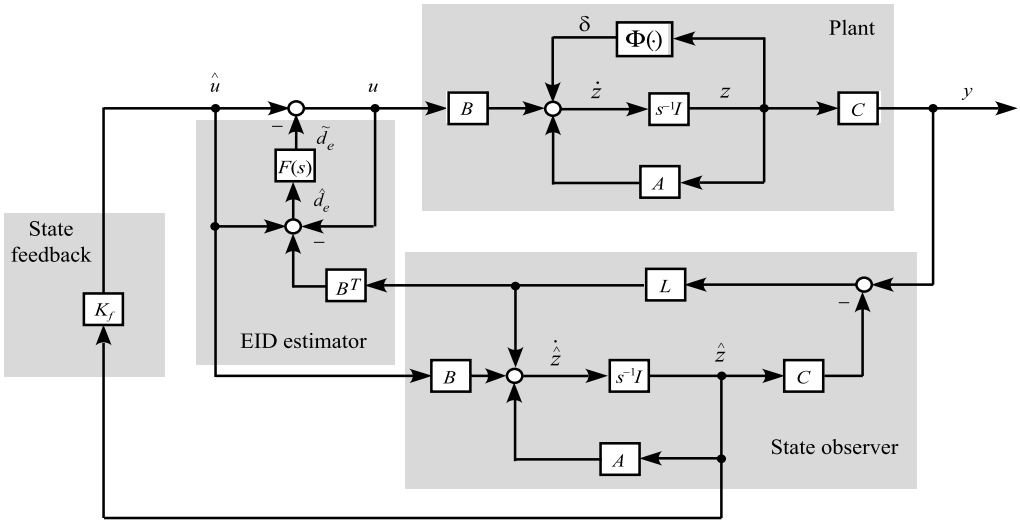

Fig. 1 Configuration of EID-based control system

A simple calculation gives us

$$C(sI_4 - A)^{-1}B = \begin{bmatrix} \frac{N_1(s)}{\Delta(s)} \\ \frac{N_2(s)}{\Delta(s)} \end{bmatrix} \tag{22}$$

where I_4 is a 4×4 identity matrix, and

$$\begin{cases} \Delta(s) = s^2[s^2 - a_{12}a_{21}] \\ N_1(s) = a_{14}s^2 + a_{12}a_{23} \\ N_2(s) = s^2 - a_{12}a_{21} \end{cases} \tag{23}$$

So, the Smith–MacMillan canonical form of the rational fraction matrix $C(sI_4 - A)^{-1}B$ is $[1/\Delta(s), 0]^T$. Thus, the system (A, B, C) has no zero. In addition, from (19), (20), and (21), we have

$$O = \begin{bmatrix} C \\ CA \end{bmatrix} = \begin{bmatrix} 1 & 0 & 0 & 0 \\ 0 & 0 & 1 & 0 \\ 0 & a_{12} & 0 & a_{14} \\ 0 & 0 & 0 & 1 \end{bmatrix}$$

Clearly, (C, A) is observable. In this study, we make the assumption

$$\left[\frac{m_{12}(q)}{m_{11}(q)}\frac{\partial G_1(q)}{\partial q_1} - \frac{\partial G_1(q)}{\partial q_2}\right]\Big|_{q=0} \neq 0 \tag{A1}$$

It is not difficult to verify that (A, B) is controllable if and only if (A1) holds.

Now, we take the nonlinear part, δ, to be an artificial state-dependent disturbance of the system (18). Since (A, B, C) is controllable and observable, and since it has no zero on the imaginary axis, as discussed in [25], there always exists an EID, d_e, on the control input channel; and we can write the plant as

$$\begin{cases} \dot{z} = Az + B(u + d_e) \\ y = Cz \end{cases} \tag{24}$$

where the EID, d_e, produces the same effect on the output as δ does. In other words, the output of (24) is the same as that of (18). Note that we abuse the notation a bit and use the same variable, z, for the state of (18) and that of (24). This should not cause confusion.

The EID-based control system for (18) that we constructed (Fig. 1) consists of four parts: the plant, an EID estimator, a state-feedback controller, and a state observer. How to design the last three parts is explained below.

4.1 Design of EID estimator

This subsection describes the design of an estimator that produces an estimate of d_e in a real-time fashion.

A full-order Luenberger state observer is used to estimate the state of the plant (24):

$$\dot{\hat{z}} = A\hat{z} + B\hat{u} + L(y - C\hat{z}) \tag{25}$$

where $\hat{u} = u + d_e$ and L is the observer gain that stabilizes $A - LC$ (see Sect. 4.3 regarding the design).

Taking the error state to be

$$\Delta z = \hat{z} - z \tag{26}$$

and substituting it into (24) yields

$$\dot{\hat{z}} = A\hat{z} + Bu + Bd_e + (\Delta\dot{z} - A\Delta z) \tag{27}$$

We find a Δd that satisfies

$$\Delta\dot{z} - A\Delta z = B\Delta d \tag{28}$$

Combining (27) and (28) yields

$$\dot{\hat{z}} = A\hat{z} + B\left(u + \hat{d}_e\right) \tag{29}$$

where

$$\hat{d}_e = d_e + \Delta d \tag{30}$$

From (25) and (29), we have

$$B\left(u + \hat{d}_e - \hat{u}\right) = L(y - C\hat{z}) \tag{31}$$

Solving (31) yields a solution for $\hat{d}_e$:

$$\hat{d}_e = B^T L(y - C\hat{z}) + \hat{u} - u \tag{32}$$

We take $\hat{d}_e$ to be an estimate of the actual EID, d_e. To ensure the estimation accuracy, we use a low-pass filter,

$$F(s) = \frac{1}{Ts + 1} \tag{33}$$

to select the frequency band for the estimate, where T is the time constant of the filter. The filtered disturbance estimate is

$$\tilde{d}_e(t) = \mathcal{L}^{-1}\left[F(s)\hat{D}_e(s)\right] \tag{34}$$

where, for any variable $\theta(t)$, $\Theta(s) = \mathcal{L}[\theta(t)]$, $\mathcal{L}[\cdot]$ is the Laplace transform, and $\mathcal{L}^{-1}[\cdot]$ is the inverse Laplace transform.

Remark 1 Since $A - LC$ is stable, $\Delta z \to 0$ as $t \to \infty$. Equations (28) and (30) show that the estimated EID, $\hat{d}_e$, asymptotically converges to its actual value, d_e.

4.2 Design of state-feedback controller

Designing the state-feedback controller for the system (24) by minimizing

$$J_K = \int_0^\infty \left\{z^T(t)Qz(t) + \hat{u}^T(t)R\hat{u}(t)\right\} dt \tag{35}$$

gives us

$$\hat{u} = K_f\hat{z}, \quad K_f = -R^{-1}B^T P \tag{36}$$

where $P = P^T$ is a positive solution of the Riccati equation

$$A^T P + PA - PBR^{-1}B^T P + Q = 0 \tag{37}$$

and $Q \geq 0$ and $R > 0$ are two given matrices. Since (A, B) is controllable and since the observer (25) is stable (see next subsection), the linear quadratic regulation (LQR) optimal control law, (36), makes the output of the plant (24) asymptotically converge to zero. As a result, according to the definition of EID, the control law

$$u = \hat{u} - \tilde{d}_e \tag{38}$$

asymptotically stabilizes the output of the plant (18) at the origin. So, the global, asymptotic stabilization of the plant (18) at the origin is guaranteed under (38).

Remark 2 Equation (14) shows that the velocity, $\dot{q}$, is necessary to deduce the control input τ_2. Since we do not measure $\dot{q}$ and since the observer (25) is asymptotically stable, we use (6) and the observer information to obtain the velocities

$$\dot{q}_1 = \frac{\hat{z}_2 - m_{12}(q)\hat{z}_4}{m_{11}(q)}, \qquad \dot{q}_2 = \hat{z}_4 \tag{39}$$

4.3 Design of state observer

The observer has two functions:

(1) to reproduce the state of the plant, which enables a state feedback control law to be constructed; and
(2) to produce an EID, which enables the non-linearities of the plant to be compensated for.

For the observer to carry them out, the observer gain, L, must be such that the observer converges faster than

the plant. The method of designing a high-gain observer in [25] is also used in this study. A brief description of the design procedure is given to make the paper self-contained.

Consider the dual-system of the linear plant:

$$\begin{cases} \frac{dz_L}{dt} = A^T z_L + C^T u_L \\ y_L = B^T z_L \end{cases} \tag{40}$$

We introduce the parameterized performance index

$$J_L = \int_0^\infty \left\{ \rho z_L^T(t) Q_L z_L(t) + u_L^T(t) R_L u_L(t) \right\} dt \tag{41}$$

for (40), where $Q_L > 0$ and $R_L > 0$ are weighting matrices, and $\rho > 0$ is a scalar parameter. The optimal observer gain is

$$\begin{cases} L = K_\rho^T \\ K_\rho = \frac{1}{2} R_L^{-1} C S \\ AS + SA^T - SC^T R_L^{-1} C S + \rho Q_L = 0 \end{cases} \tag{42}$$

From (42), we have

$$(A - LC)\, S + S\,(A - LC)^T + \rho Q_L = 0 \tag{43}$$

That means that L designed in (42) stabilizes $A - LC$ and a larger ρ makes the observer dynamics quicker [27]. In addition [28],

$$\lim_{\rho \to \infty} \left[sI - (A - LC) \right]^{-1} B = 0 \tag{44}$$

4.4 Stability of EID-based control system

Now, let us consider the stability of the EID-based control system. Since the dynamics of the high-gain observer converge much more quickly than those of the plant, an EID can quickly be estimated. This enables the non-linearities to be quickly compensated for. Under the condition that the non-linearities are completely compensated for by the EID, we can take $d_e = 0$ when discussing the stability issue. Combining (25), (27), and (38) yields

$$\Delta \dot{z} = (A - LC)\Delta z + B \tilde{d}_e \tag{45}$$

From (26), (32), and (38), we have

$$\hat{d}_e = -B^T LC \Delta z + \tilde{d}_e \tag{46}$$

The transfer function from $\tilde{d}_e$ to $\hat{d}_e$ is derived from (41) and (42):

$$\begin{aligned} G_L(s) &= 1 - B^T LC \left[sI - (A - LC) \right]^{-1} B \\ &= B^T (sI - A) \left[sI - (A - LC) \right]^{-1} B \end{aligned} \tag{47}$$

The separation theorem [25] and small-gain theorem [29] tell us that the stability of the whole system is guaranteed under the following conditions:

C1: $A + BK_f$ and $A - LC$ are stable.

C2: $\|G_L F\|_\infty = \sup_{\omega \geq 0} \sigma_{\max} \left[G_L(j\omega) F(j\omega) \right] < 1$

where $\sigma_{\max}[\cdot]$ is the maximum singular-value function.

From (36), (37), and (43), it is easy to verify that condition C1 is true. In addition, since the left side of (44) is part of $G_L(s)$, for a given filter, $F(s)$, condition C2 is guaranteed by the L designed in (42) for a large enough ρ.

5 Numerical examples

We employed the above method to globally stabilize three kinds of 2-DOF underactuated mechanical systems: a TORA, a beam–ball system, and an inertia wheel pendulum. The simulation results demonstrate the validity of the method. Note that, as shown in (20), the matrices B and C are the same for all the systems. So, we only discuss the matrix A below.

5.1 TORA system

A TORA (Fig. 2) consists of a cart and an eccentric rotational proof mass. The cart moves horizontally along a line and is connected to a wall by a spring. The proof mass is attached to the cart and is actuated by a DC motor. q_1 is the translational position of the cart, and q_2 is the rotational angle of the proof mass. We assume that there are no external disturbances on the cart. The dynamics of a TORA are [30]

$$M(q_2) \begin{bmatrix} \ddot{q}_1 \\ \ddot{q}_2 \end{bmatrix} + \begin{bmatrix} -m_2 r \dot{q}_2^2 \sin q_2 \\ 0 \end{bmatrix} + \begin{bmatrix} kq_1 \\ 0 \end{bmatrix} = \begin{bmatrix} 0 \\ \tau_2 \end{bmatrix} \tag{48}$$

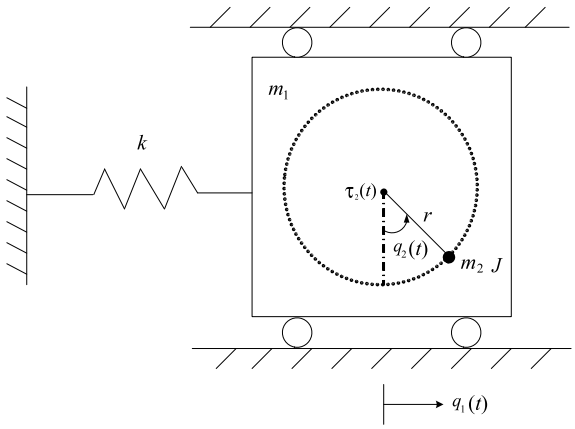

Fig. 2 Model of TORA

where

$$M(q_2)=\begin{bmatrix} m_1+m_2 & m_2 r\cos q_2 \\ m_2 r\cos q_2 & m_2 r^2+J \end{bmatrix}$$

m_1 is the mass of the cart, m_2 is the mass of the proof mass, r is the rotary radius of the proof mass, J is the moment of inertia of the proof mass, k is a spring constant, and τ_2 is the control torque that drives the proof mass. It is not difficult to verify that Assumption (A1) is satisfied for (48). Clearly, the TORA is an example of USSV-A. We have taken

$$\alpha(q_2)=\int_0^{q_2}\frac{m_2 r\cos v}{m_1+m_2}\,dv=\frac{m_2 r}{m_1+m_2}\sin q_2$$

in the transformation $\mathcal{T}$ in (6). Then $\mathcal{T}$ becomes

$$\mathcal{T}:\ \begin{cases} z_1=q_1+\frac{m_2 r}{m_1+m_2}\sin q_2 \\ z_2=(m_1+m_2)\dot q_1+m_2 r\dot q_2\cos q_2 \\ z_3=q_2 \\ z_4=\dot q_2 \end{cases} \tag{49}$$

It transforms the system (48) into

$$\begin{cases} \dot z_1=\frac{z_2}{m_1+m_2} \\ \dot z_2=-kz_1+\lambda\sin z_3, \quad \lambda=\frac{km_2 r}{m_1+m_2} \\ \dot z_3=z_4 \\ \dot z_4=u \end{cases} \tag{50}$$

From (19), (21), and (48), we have

$$A=\begin{bmatrix} 0 & \frac{1}{m_1+m_2} & 0 & 0 \\ -k & 0 & \lambda & 0 \\ 0 & 0 & 0 & 1 \\ 0 & 0 & 0 & 0 \end{bmatrix},\qquad \delta=\begin{bmatrix} 0 \\ \lambda(\sin z_3-z_3) \\ 0 \\ 0 \end{bmatrix} \tag{51}$$

Consider the TORA system

$$\begin{cases} m_1=4.9\ \text{kg}, \quad m_2=0.1\ \text{kg}, \quad r=0.8\ \text{m} \\ J=0.064\ \text{kg}\cdot\text{m}^2, \quad k=350\ \text{N/m} \end{cases} \tag{52}$$

The design parameters for (33), (35), and (41) were chosen to be

$$\begin{cases} Q=I_4, \quad R=0.01, \quad T=0.2 \\ Q_L=I_4, \quad R_L=1000I_2, \quad \rho=10^8 \end{cases} \tag{53}$$

Then, using the functions `lqr`, `eig`, and `norm` in MATLAB yields

$$K_f=\begin{bmatrix} 359.5550 & 5.1169 & -15.7542 & -11.4677 \end{bmatrix} \tag{54}$$

$$L=\begin{bmatrix} 158.1524 & 60.8661 & 0.0009 & -0.0005 \\ 0.0009 & 2.8007 & 158.6131 & 158.1139 \end{bmatrix}^T \tag{55}$$

Eigenvalues of $(A+BK_f)$

$$=-9.9549,-1.0020,-0.2554\pm 8.3736i \tag{56}$$

Eigenvalues of $(A-LC)$

$$=-157.6313,-157.6097,-1.0032,-0.5213 \tag{57}$$

$$\|G_L F\|_\infty=0.8354<1 \tag{58}$$

In [30, 31], the variables

$$\begin{cases} x_d=\sqrt{\frac{m_1+m_2}{J+m_2r^2}}q_1, \quad \theta=q_2, \quad \upsilon=\sqrt{\frac{k}{m_1+m_2}}t \\ \varepsilon=\frac{m_2 r}{\sqrt{(J+m_2r^2)(m_1+m_2)}}, \quad U=\frac{m_1+m_2}{k(J+m_2r^2)}\tau_2 \end{cases} \tag{59}$$

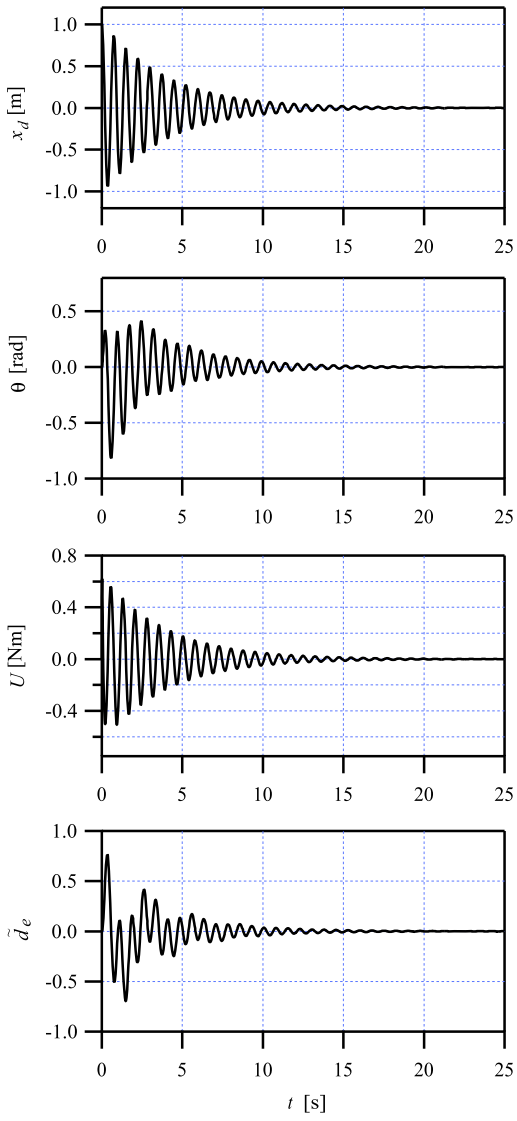

Fig. 3 Simulation results for TORA

were introduced to simplify the description of a TORA. That gives us

$$\begin{cases} \frac{dx_d}{d\upsilon} = \frac{dx_d}{dt}\frac{dt}{d\upsilon} = \frac{m_1+m_2}{\sqrt{k(J+m_2r^2)}}\dot{q}_1 \\ \frac{d\theta}{d\upsilon} = \frac{d\theta}{dt}\frac{dt}{d\upsilon} = \sqrt{\frac{m_1+m_2}{k}}\dot{q}_2 \end{cases} \tag{60}$$

To compare our results with theirs, these variables were also used in our simulations. We took the initial condition of the simulations to be

$$\begin{aligned} &\left[q_1, q_2, \dot{q}_1, \dot{q}_2\right]^T \\ &= \left[\sqrt{\left(J+m_2r^2\right)/(m_1+m_2)}, 0, 0, 0\right]^T \end{aligned} \tag{61}$$

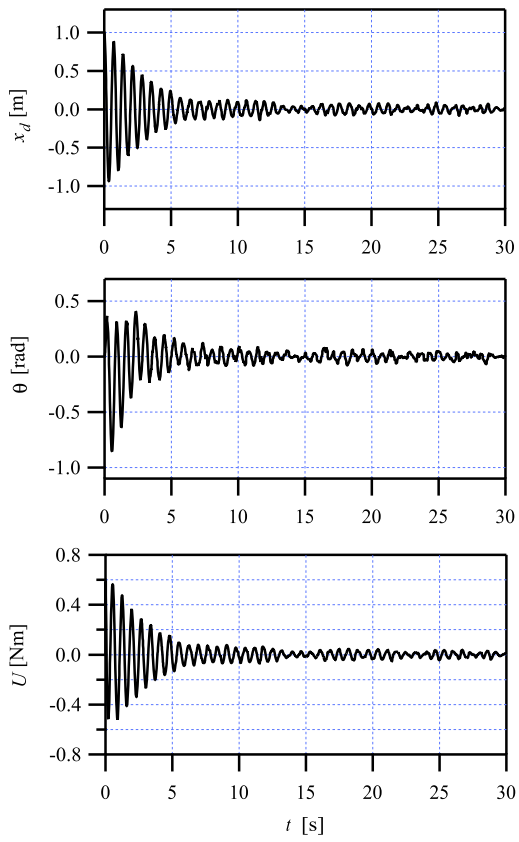

Fig. 4 Simulation results for TORA for the case where m_1 is 10% smaller than its nominal value, m_2 and J are 10% larger than their nominal values, and there is white noise (peak value: ± 0.05) in the measured q

From (52), (59), (60), and (61), we obtain $\varepsilon = 0.1$ and

$$[x_d, \theta, dx_d/d\upsilon, d\theta/d\upsilon]^T = [1, 0, 0, 0]^T$$

which were used in [30, 31]. Figure 3 shows the time responses of x_d, θ, U, and the filtered EID, $\tilde{d}_e$. The results show that the settling time is about 15 s, and the largest value of U is about 0.6 Nm. In contrast, the settling time is longer than 25 s in [30] and over 35 s in [31], and the largest value of U is greater than 6 Nm in [30] and greater than 3 Nm in [31]. Moreover, both of those methods require q and $\dot{q}$ to design the control law. So, our method requires fewer measurement variables and smaller control torques, and yields a faster response.

To verify the robustness of our method, we carried out simulations with parameter uncertainties for the designed control system. Figure 4 shows the results for the case where m_1 is 10% smaller than its nominal

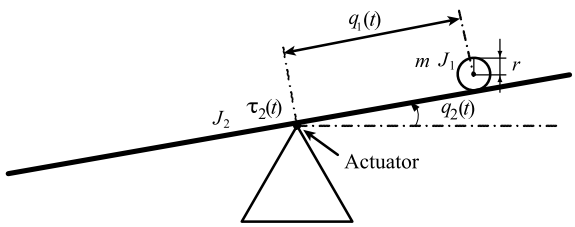

Fig. 5 Model of beam–ball system

value, m_2 and J are 10% larger than their nominal values, and there is white noise (peak value: ± 0.05) in the measured q. Clearly, the system is stable when there are parameter uncertainties and measurement noise, and our control strategy is practical.

5.2 Beam–ball system

A beam–ball system (Fig. 5) consists of a ball that rolls along a beam and an actuator that tilts the beam to move the ball. Let q_1 be the position of the ball, and q_2 be the angle of the beam. The dynamics of the beam–ball are

$$\begin{aligned} &M(q_1)\begin{bmatrix}\ddot{q}_1\\ \ddot{q}_2\end{bmatrix}+\begin{bmatrix}-mq_1\dot{q}_2^2\\ 2mq_1\dot{q}_1\dot{q}_2\end{bmatrix}+\begin{bmatrix}mg\sin q_2\\ mgq_1\cos q_2\end{bmatrix}\\ &\quad=\begin{bmatrix}0\\ \tau_2\end{bmatrix}\\ &M(q_1)=\begin{bmatrix}m\lambda & 0\\ 0 & mq_1^2+J_2\end{bmatrix}\end{aligned} \tag{62}$$

where $\lambda = 1 + J_1/mr^2$, m is the mass of the ball, r is the radius of the ball, J_1 is the moment of inertia of the ball, J_2 is the moment of inertia of the beam, $g\ (= 9.80665\ \text{m/s}^2)$ is the gravitational constant, and τ_2 is the torque applied to the beam. It is easy to verify that Assumption (A1) is satisfied for (62).

Since the beam–ball system is an example of USSV-U, we take $\alpha(q_2) = 0$ in (6) and obtain the following coordinate transformation for (62):

$$z_1 = q_1, \quad z_2 = m\lambda\dot{q}_1, \quad z_3 = q_2, \quad z_4 = \dot{q}_2 \tag{63}$$

It converts the system (62) into

$$\begin{cases}\dot{z}_1 = \frac{z_2}{m\lambda}\\ \dot{z}_2 = -mg\sin z_3 + mz_1z_4^2\\ \dot{z}_3 = z_4\\ \dot{z}_4 = u\end{cases} \tag{64}$$

Table 1 Mechanical parameters of beam–ball

m [kg]	r [m]	J_1 [kg·m^2]	J_2 [kg·m^2]
0.05	0.01	2×10^{-6}	0.02

Equations (19), (21), and (62) yield

$$\begin{aligned} A &= \begin{pmatrix}0 & \frac{1}{m\lambda} & 0 & 0\\ 0 & -\beta & -mg & 0\\ 0 & 0 & 0 & 1\\ 0 & 0 & 0 & 0\end{pmatrix},\\ \delta &= \begin{pmatrix}0\\ -mg[\sin z_3 - z_3] + mz_1z_4^2\\ 0\\ 0\end{pmatrix}\end{aligned} \tag{65}$$

The mechanical parameters of the beam–ball in [32] (Table 1) were used for simulations. And the design parameters were chosen to be

$$\begin{cases}Q = I_4, \quad R = 0.05, \quad T = 0.1\\ Q_L = 0.5I_4, \quad R_L = 100I_2, \quad \rho = 10^8\end{cases} \tag{66}$$

That produced

$$K_f = \begin{bmatrix}4.4721 & 80.5763 & -24.8381 & -8.3472\end{bmatrix} \tag{67}$$

$$L = \begin{bmatrix}360.6255 & 353.5535 & -0.0024 & -0.0021\\ -0.0024 & -0.2431 & 354.0530 & 353.5534\end{bmatrix}^T \tag{68}$$

Eigenvalues of $(A + BK_f)$

$$= -4.3362, -2.1044, -0.9534 \pm 1.5888i \tag{69}$$

Eigenvalues of $(A - LC)$

$$= -353.0516, -353.0516, -14.5964, -1.0014 \tag{70}$$

$$\|G_L F\|_\infty = 0.9116 < 1 \tag{71}$$

For the initial condition

$$\begin{bmatrix}q_1, q_2, \dot{q}_1, \dot{q}_2\end{bmatrix}^T = [0, \pi/3, 0, 0]^T \tag{72}$$

Fig. 6 shows the simulation results. The filtered EID, $\tilde{d}_e$ is also shown in the figure.

The settling time of the beam–ball system is about 10 s, which is as good as that in [33], in which both the position and velocity are required. However, the

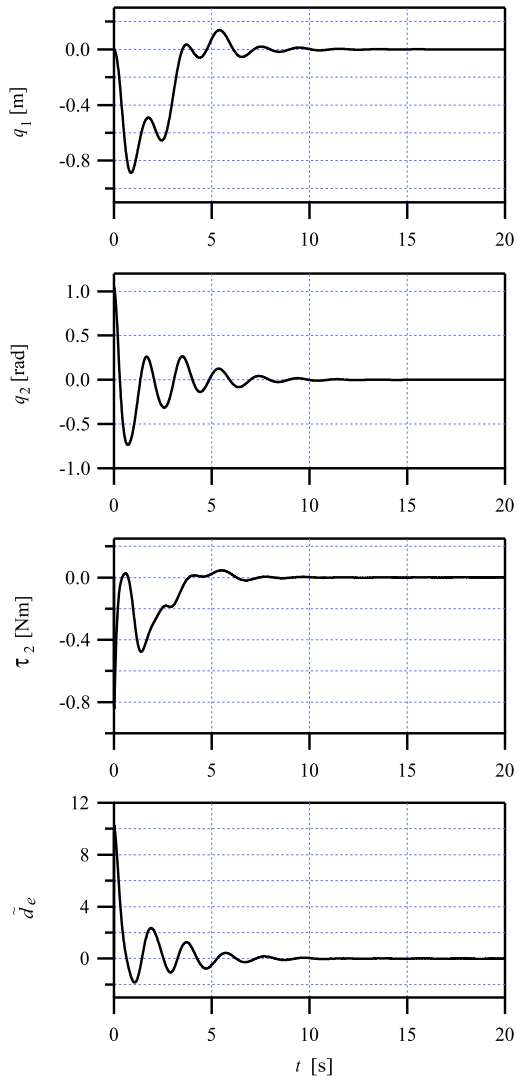

Fig. 6 Simulation results for beam–ball system

largest control input in Fig. 6 is less than 1 Nm, while it is greater than 3 Nm in [33]. Clearly, our method requires fewer measurement variables and a lower control torque than [33] does.

For the designed control system, we studied the problem of robustness through simulations. Figure 7 shows the results for the case where m and J_1 are 10% larger than their nominal values, J_2 is 10% smaller than its nominal value, and there is white noise (peak value: ± 0.1) in the measured q. The results show that the EID-based strategy is effective even under these conditions.

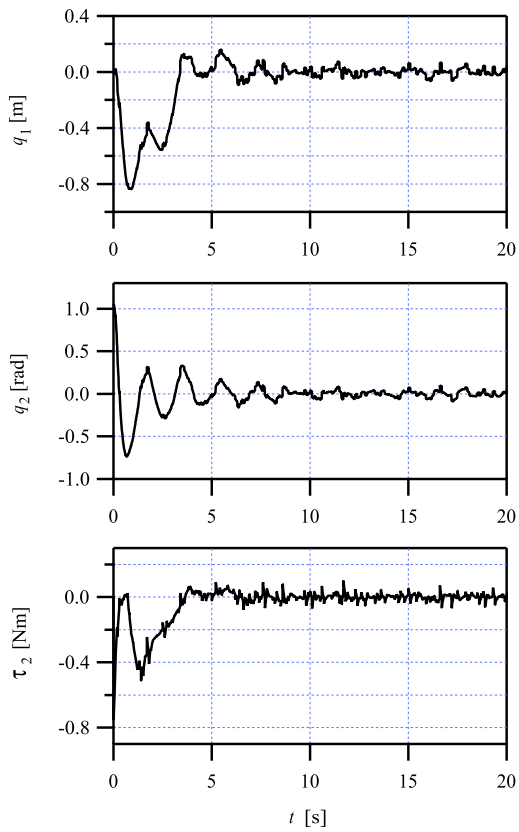

Fig. 7 Simulation results for beam–ball system for the case where m and J_1 are 10% larger than their nominal values, J_2 is 10% smaller than its nominal value, and there is white noise (peak value: ± 0.1) in the measured q

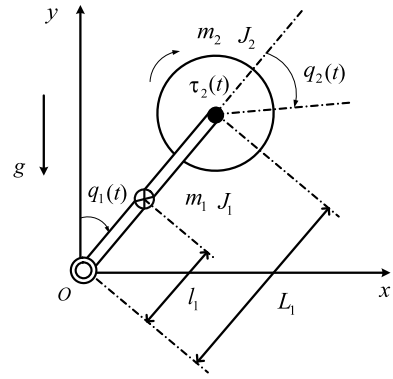

Fig. 8 Model of inertia wheel pendulum

5.3 Inertia wheel pendulum

An inertia wheel pendulum (Fig. 8) consists of a pendulum with a rotating uniform inertia wheel attached

Table 2 Parameters of inertia wheel pendulum

m_1 [kg]	L_1 [m]	l_1 [m]	m_2 [kg]	J_1 [kg·m^2]	J_2 [kg·m^2]
0.02	0.125	0.063	0.3	47×10^{-6}	32×10^{-6}

to the end. The wheel is actuated by a motor and spins about an axis parallel to the axis of rotation of the pendulum. The joint at the base is unactuated. The pendulum is controlled by means of the coupling torque produced by rotation of the wheel. q_1 and q_2 are the angular positions of the pendulum and wheel, respectively. The dynamics of the system are [34]

$$M\begin{bmatrix}\ddot{q}_1\\ \ddot{q}_2\end{bmatrix}+\begin{bmatrix}-m_0\sin q_1\\ 0\end{bmatrix}=\begin{bmatrix}0\\ \tau_2\end{bmatrix} \tag{73}$$

where

$$M=\begin{bmatrix}m_{11} & m_{12}\\ m_{21} & m_{22}\end{bmatrix}=\begin{bmatrix}m_1l_1^2+m_2L_1^2+J_1+J_2 & J_2\\ J_2 & J_2\end{bmatrix}$$

$$m_0=(m_1l_1+m_2L_1)\,g$$

m_1 is the mass of the pendulum, L_1 is its length, J_1 is its moment of inertia, l_1 is the distance from the first joint to the center of mass of the pendulum, m_2 is the mass of the wheel, J_2 is its moment of inertia, and τ_2 is the control torque applied to the wheel. Clearly, Assumption (A1) is satisfied for (73).

The inertia wheel pendulum is an example of USCIM. We took $\alpha(q_2)=0$ in (6) and chose the coordinate transformation to be

$$\mathcal{T}:\quad\begin{cases}z_1=q_1\\ z_2=m_{11}\dot{q}_1+m_{12}\dot{q}_2\\ z_3=q_2\\ z_4=\dot{q}_2\end{cases} \tag{74}$$

That gives the dynamics of the system in the z-state

$$\begin{cases}\dot{z}_1=\frac{1}{m_{11}}z_2-\frac{m_{12}}{m_{11}}z_4\\ \dot{z}_2=m_0\sin z_1\\ \dot{z}_3=z_4\\ \dot{z}_4=u\end{cases} \tag{75}$$

Combining (19), (21), and (73) yields

$$A=\begin{pmatrix}0 & \frac{1}{m_{11}} & 0 & -\frac{m_{12}}{m_{11}}\\ m_0 & 0 & 0 & 0\\ 0 & 0 & 0 & 1\\ 0 & 0 & 0 & 0\end{pmatrix},\qquad \delta=\begin{pmatrix}0\\ m_0[\sin z_1-z_1]\\ 0\\ 0\end{pmatrix} \tag{76}$$

We used the inertia wheel pendulum system in [35] (Table 2) and chose the design parameters to be

$$\begin{cases}Q=0.5I_4, & R=0.5, \quad T=0.5\\ Q_L=0.05I_4, & R_L=10^5I_2, \quad \rho=10^8\end{cases} \tag{77}$$

That yielded

$$K_f=\begin{bmatrix}302.3073 & 5477.5583 & 1.0000 & -15.5057\end{bmatrix} \tag{78}$$

$$L=\begin{bmatrix}21.8639 & 3.7307 & -0.0004 & 0.0112\\ -0.0004 & -0.0112 & 4.0044 & 3.5355\end{bmatrix}^T \tag{79}$$

Eigenvalues of $(A+BK_f)$

$$=-6.8871\pm0.0292i,\ -0.8660\pm0.4999i \tag{80}$$

Eigenvalues of $(A-LC)$

$$=-10.9320\pm17.2798i,\ -2.6902,\ -1.3142 \tag{81}$$

$$\|G_LF\|_\infty=0.8336<1 \tag{82}$$

For the initial condition

$$\begin{bmatrix}q_1, q_2, \dot{q}_1, \dot{q}_2\end{bmatrix}^T=[\pi,0,0,0]^T \tag{83}$$

Fig. 9 shows the simulation results as well as the filtered EID, $\tilde{d}_e$. It is clear that our method makes the system quickly converge to the origin, regardless of the state. The control performance is as good as those reported in [9]; but that method requires measurements of both q and $\dot{q}$, and it does not guarantee the convergence of q_2.

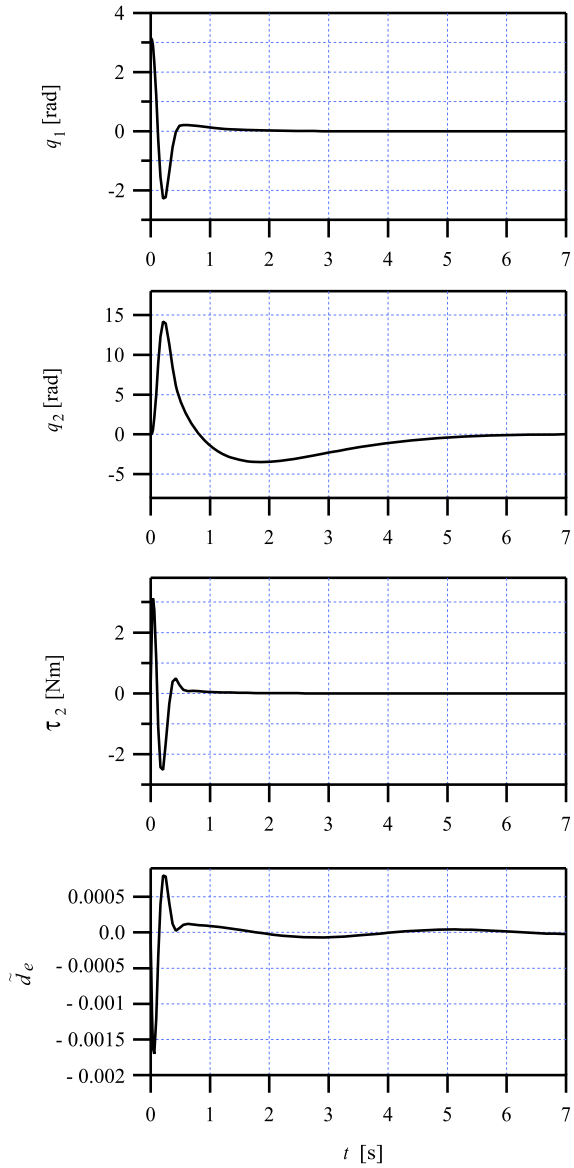

Fig. 9 Simulation results for inertia wheel pendulum

In addition, we considered the robustness of the control system when parameter uncertainties and measurement noise are present. Figure 10 shows the simulation results for the case where m_1, l_1, and J_1 are 10% larger than their nominal values, m_2 and J_2 are 10% smaller than their nominal values, and there is white noise (peak value: ± 0.1) in the measured q. It is clear that the EID-based strategy is still effective under these conditions.

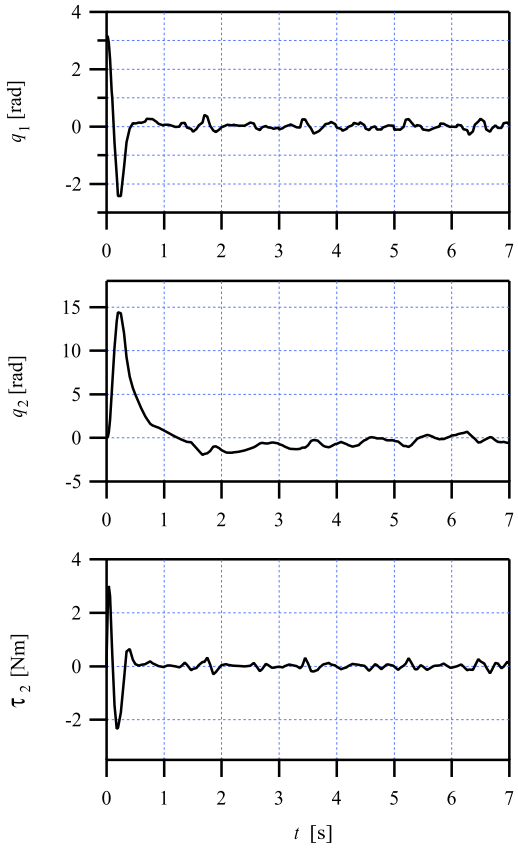

Fig. 10 Simulation results for inertia wheel pendulum for the case where m_1, l_1, and J_1 are 10% larger than their nominal values, m_2 and J_2 are 10% smaller than their nominal values, and there is white noise (peak value: ± 0.1) in the measured q

6 Conclusion

This paper presents a new method of stabilizing a 2-DOF underactuated mechanical system that is based on the concept of EID. It has the advantage of requiring only positional information for the design of a control law. To globally asymptotically stabilize a system at the origin, we utilize the general momentum associated with the variables of the unactuated part and carry out a homeomorphic global coordinate transformation on the system, thereby converting it into a new one that is easy to handle. This changes the problem of stabilizing the original system into one of stabilizing the new system. Then an EID-based control law is designed that globally asymptotically stabilizes the new system at the origin. This method was applied to the control of three well-known 2-DOF underactuated mechanical systems: a TORA, a beam–ball system, and an inertia

wheel pendulum. Simulations demonstrated the validity of the method and its superiority over others.

In addition, it is easy to generalize our method to the stabilization of an n-DOF ($n \geq 3$) underactuated mechanical system.

Acknowledgements This work was supported in part by the National Science Foundation of China under Grants 61074112 and 60974045.

References

1. Bullo, F., Lynch, K.M.: Kinematic controllability for decoupled trajectory planning in underactuated mechanical systems. IEEE Trans. Robot. Autom. **17**(4), 402–412 (2001)
2. Grizzle, J.W., Moog, C.H., Chevallereau, C.: Nonlinear control of mechanical systems with an unactuated cyclic variable. IEEE Trans. Autom. Control **50**(5), 559–576 (2005)
3. Blajer, W., Kołodziejczyk, K.: Control of underactuated mechanical systems with servo-constraints. Nonlinear Dyn. **50**(4), 781–791 (2007)
4. Alleyne, A.: Physical insights on passivity-based TORA control designs. IEEE Trans. Control Syst. Technol. **6**(3), 436–439 (1998)
5. Albahkali, T., Mukherjee, R.: Das T.: Swing-up control of the pendubot: An impulse-momentum approach. IEEE Trans. Robot. **25**(4), 975–982 (2009)
6. Lai, X., She, J., Yang, S.X., Wu, M.: Control of acrobot based on non-smooth Lyapunov function and comprehensive stability analysis. IET Control Theory Appl. **2**(3), 181–191 (2008)
7. Almutairi, N.B., Zribi, M.: On the sliding mode control of a ball on a beam system. Nonlinear Dyn. **59**(1–2), 221–238 (2010)
8. Ibanez, C., Azuela, J.: Stabilization of the Furuta pendulum based on a Lyapunov function. Nonlinear Dyn. **49**(1–2), 1–8 (2007)
9. Praly, L., Ortega, R., Kaliora, G.: Stabilization of nonlinear systems via forwarding *modLgV*. IEEE Trans. Autom. Control **46**(9), 1461–1466 (2001)
10. Oriolo, G., Nakamura, Y.: Control of mechanical systems with second-order nonholonomic constraints: underactuated manipulators. In: Proc. 30th IEEE Conference on Decision and Control, Brighton, UK, pp. 2398–2403 (1991)
11. Fantoni, I., Lozano, R., Spong, M.W.: Energy based control of the pendubot. IEEE Trans. Autom. Control **45**(4), 725–729 (2000)
12. Lai, X., She, J., Yang, S.X., Wu, M.: Comprehensive unified control strategy for underactuated two-link manipulators. IEEE Trans. Syst. Man Cybern., Part B, Cybern. **39**(2), 389–398 (2009)
13. Xin, X., Kaneda, M.: Analysis of the energy-based swing-up control of the Acrobot. Int. J. Robust Nonlinear Control **17**(16), 1503–1524 (2007)
14. Xin, X., Kaneda, M.: Swing-up control for a 3-DOF gymnastic robot with passive first joint: design and analysis. IEEE Trans. Robot. **23**(6), 1271–1285 (2007)
15. Khalil, H.K.: Nonlinear Systems, 3rd edn. Prentice-Hall, Englewood Cliffs (2002)
16. Spong, M.W.: The swing up control problem for the acrobot. IEEE Control Syst. Mag. **15**(1), 44–55 (1995)
17. Aoustin, Y., Formal'skii, A., Martynenko, Y.: Pendubot: combining of energy and intuitive approaches to swing up, stabilization in erected pose. Multibody Syst. Dyn. **25**(1), 60–85 (2011)
18. Seifried, R.: Two approaches for feedforward control and optimal design of underactuated multibody systems. Multibody Syst. Dyn. (2011). doi:10.1007/s11044-011-9261-z
19. Olfati-Saber, R.: Control of underactuated mechanical systems with two degrees of freedom and symmetry. In: Proc. American Control Conference, Chicago, IL, pp. 4092–4096 (2000)
20. Qaiser, N., Iqbal, N., Hussain, A., Qaiser, N.: Exponential stabilization of a class of underactuated mechanical systems using dynamic surface control. Int. J. Control. Autom. Syst. **5**(5), 547–558 (2007)
21. Ortega, R., Spong, M.W., Gómez-Estern, F., Blankenstein, G.: Stabilization of a class of underactuated mechanical systems via interconnection and damping assignment. IEEE Trans. Autom. Control **47**(8), 1218–1232 (2002)
22. Acosta, J.A., Lopez-Martinez, M.: Constructive feedback linearization of underactuated mechanical systems with 2-DOF. In: Proc. 40th IEEE Conference on Decision and Control, Seville, Spain, pp. 4909–4914 (2005)
23. Xu, R., Ozguner, U.: Sliding mode control of a class of underactuated systems. Automatica **44**(1), 233–241 (2008)
24. Berghuis, H., Nijmeijer, H.: A passivity approach to controller-observer design for robots. IEEE Trans. Robot. Autom. **9**(6), 740–754 (1993)
25. She, J., Fang, M., Ohyama, Y., Hashimoto, H., Wu, M.: Improving disturbance-rejection performance based on an equivalent-input-disturbance approach. IEEE Trans. Ind. Electron. **55**(1), 380–389 (2008)
26. Mullhaupt, Ph., Srinivasan, B., Bonvin, D.: Analysis of exclusively-kinetic two-link underactuated mechanical systems. Automatica **38**(9), 1565–1573 (2002)
27. Anderson, B.D.O., Moore, J.B.: Optimal Control: Linear Quadratic Method. Prentice-Hall, Englewood Cliffs (1989)
28. Kimura, H.: A new approach to perfect regulation and the bounded peaking in linear multivariable control systems. IEEE Trans. Autom. Control **26**(1), 253–270 (1981)
29. Zhou, K., Doyle, J.C., Glover, K.: Robust and Optical Control. Prentice-Hall, Englewood Cliffs (1996)
30. Wan, C.J., Bernstein, D.S., Coppola, V.T.: Global stabilization of the oscillating eccentric rotor. Nonlinear Dyn. **10**(1), 49–62 (1996)
31. Jankovic, M., Fontaine, D., Kokotovic, P.: TORA example: cascade- and passivity-based control designs. IEEE Trans. Control Syst. Technol. **4**(3), 292–297 (1996)
32. Hauser, J., Sastry, S., Kokotovid, P.: Nonlinear control via approximate input-output linearization: the ball and beam example. IEEE Trans. Autom. Control **37**(3), 392–398 (1992)
33. Chen, S., Yu, F., Chung, H.: Decoupled fuzzy controller design with single-input fuzzy logic. Fuzzy Sets Syst. **129**(3), 335–342 (2002)

34. Santibanez, V., Kelly, R., Sandoval, J.: Control of the inertia wheel pendulum by bounded torques. In: Proc. 44th IEEE Conference on Decision and Control, Seville, Spain, pp. 8266–8270 (2005)

35. Spong, M.W., Corke, P., Lozano, R.: Nonlinear control of the reaction wheel pendulum. Automatica **37**(11), 1845–1851 (2001)